



Glutamic acid-assisted sol–gel synthesis of multi-doped spinel lithium manganate as cathode materials for lithium rechargeable batteries

R. Thirunakaran^{a,*}, R. Ravikumar^a, S. Vanitha^b, S. Gopukumar^a, A. Sivashanmugam^a

^a Central Electrochemical Research Institute, Karaikudi 630 006, Tamil Nadu, India

^b J. J. College of Arts & Science, Pudukkottai, Tamil Nadu, India

ARTICLE INFO

Article history:

Received 25 July 2011

Received in revised form

15 September 2011

Accepted 20 September 2011

Available online 29 September 2011

Keywords:

Triple doping

Sol–gel method

Glutamic acid

Differential capacity

Spinel cathode

Li-ion battery

ABSTRACT

LiMn₂O₄ and LiMg_xSn_yAl_zMn_{2-x-y-z}O₄ ($x, y, z = \text{Mg, Sn, Al}$) ($x = 0.01–0.09$; $y = 0.04–0.1$; $z = 0.35–0.20$) powders have been synthesized via the sol–gel method for the first time using glutamic acid as the chelating agent. The synthesized samples have been subjected to physical and electrochemical characterization. SEM images of parent LiMn₂O₄ show that the majority of the grains are 1 μm in size. The LiMg_{0.01}Sn_{0.04}Al_{0.35}Mn_{1.6}O₄ and LiMg_{0.04}Sn_{0.06}Al_{0.30}Mn_{1.6}O₄ particles present a low degree of agglomeration and the primary particles are 1 μm in size. TEM images of the spinel LiMn₂O₄ and LiMg_xSn_yAl_zMn_{2-x-y-z}O₄ ascertain that the synthesized particles are nano-sized with uniform surface morphology. The LiMn₂O₄ samples calcined at 850 °C deliver a discharge capacity of 122 mAh g⁻¹ in the first cycle. Among the compositions investigated, LiMg_{0.01}Sn_{0.06}Al_{0.30}Mn_{1.6}O₄ delivers 115 mAh g⁻¹ in the first cycle and exhibits stable cycling performance with a low capacity fade of 1 mAh g⁻¹ cycle⁻¹ over the 10 cycles investigated.

© 2011 Elsevier Ltd. All rights reserved.

1. Introduction

LiMn₂O₄ is an apssite and attractive cathode material for rechargeable lithium batteries owing to its low cost, environmentally benign nature, and ease of preparation when compared with other layered oxides such as LiCoO₂ and LiNiO₂ [1–3]. However, the specific capacity of pure spinel LiMn₂O₄ decreases gradually upon repeated cycling at elevated temperature [4,5]. It is well known that capacity fading is due to several factors, including Jahn–Teller distortion, a two-phase unstable reaction [2], slow dissolution of manganese into the electrolyte [6], lattice instability [7], and particle size distribution [8]. In order to overcome the problem of Jahn–Teller distortion in obtaining high capacity retention, several researchers have investigated lithium rich spinels with various divalent, trivalent and tetravalent-doped ions such as Cr, Fe, Zn, Cu, Ga, Co, Al, Ni and Ti [9]. Song et al [8] and Lee et al. [10] have reported that the partial doping of cations is effective in suppressing capacity fade upon cycling. Moreover, the capacity fade of LiMn₂O₄ often occurs in the 3 V region and can be completely suppressed by doping selenium with LiMn₂O₄ [11]. Low temperature synthesis methods such as sol–gel [12,13], chemical precipitation [14], and hydrothermal and pechini processes [15] have been used to obtain

cathode materials with the expected physical and electrochemical properties for use in lithium-ion batteries. The work reported here is the first attempt to stabilize the spinel structure by using glutamic acid as a chelating agent with tri-cation doping, specifically LiMg_xSn_yAl_zMn_{2-x-y-z}O₄ ($x, y, z = \text{Mg, Sn, Al}$) ($x = 0.01–0.09$; $y = 0.04–0.1$; $z = 0.35–0.20$), synthesized through a sol–gel process.

Further, the dopant ions are in the oxidation state of Mg²⁺, Sn²⁺ and Al³⁺ in this spinel compound. Mg doping in the spinel structure has been found to be beneficial [16] due to the large ionic radius (7.2 nm) of Mg²⁺ ions which stand as pillars in facilitating easy lithium ion mobility into 8a tetrahedra. Studies on Sn-doped LiMn₂O₄ are scarce. However, in a study [17] of Sn⁴⁺ doped on LiMn₂O₄ synthesized via precipitation, it has been reported that Sn diffuses into the spinel lattice due to the higher bonding energy of Sn–O and the shorter bonding length of Sn–O compared to Mn–O, which makes the crystal structure more stable, leading to the stable cycling performances of Sn-doped LiMn₂O₄ cathodes during the charge–discharge process. Al-doping in LiMn₂O₄ helps in the charge compensation of Mn³⁺ ions and subdues the Jahn–Teller distortion [18]. Furthermore, the fact that both Sn²⁺ and Al³⁺ counterparts have similar ionic radii (0.69 and 5.9 nm) may be beneficial in combination with the former in stabilizing the effect of Sn²⁺ on the spinel structure. On the other hand, the triple doping enables charge balance with the charge of the Mn³⁺/Mn⁴⁺ couple. Therefore, the combined effect of triple doping in the Mn-spinel is expected to enhance the electrochemical performance of LiMn₂O₄.

* Corresponding author. Fax: +91 4565 227779.

E-mail address: rthirunakaran@yahoo.com (R. Thirunakaran).

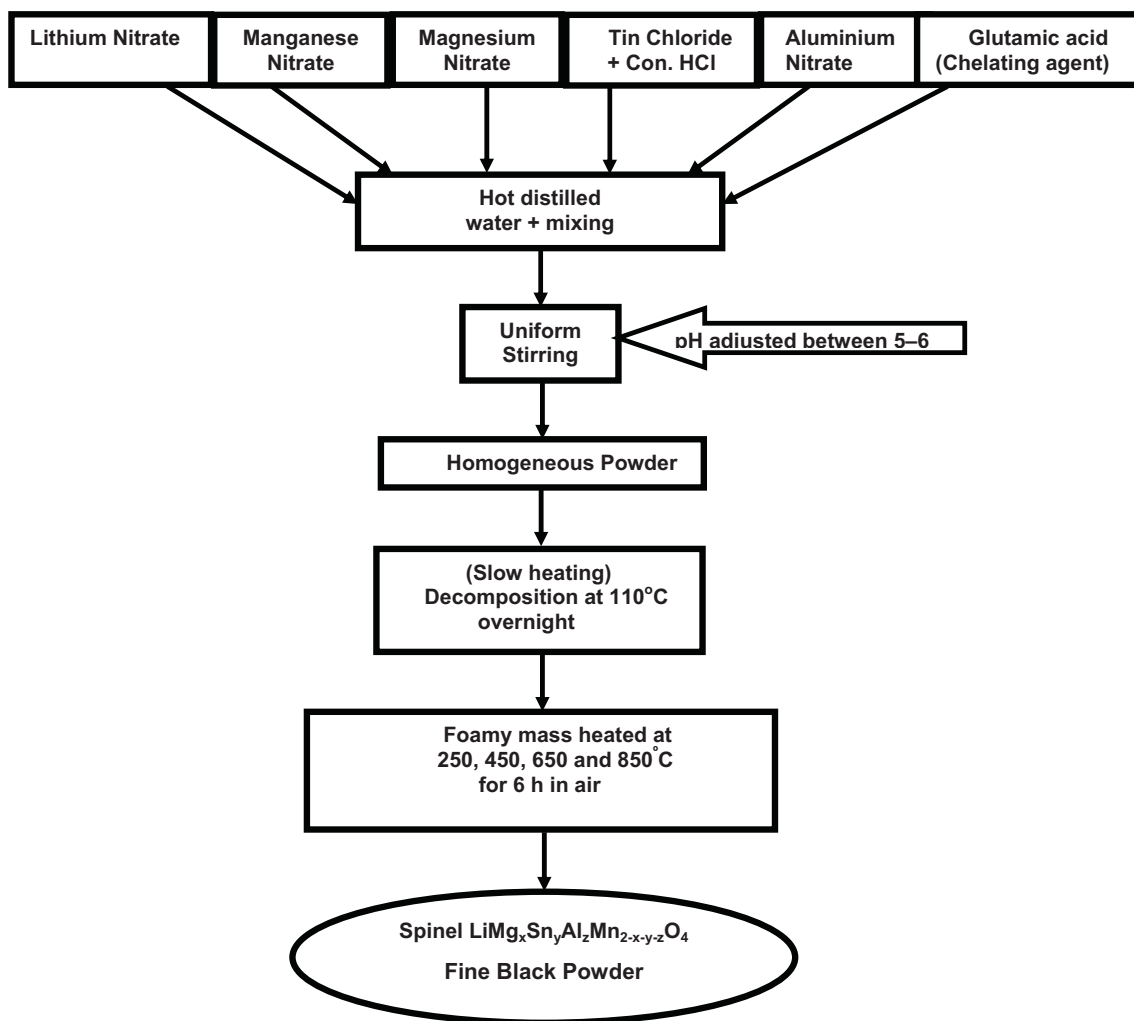


Fig. 1. Flow chart of the synthesis of $\text{LiMg}_x\text{Sn}_y\text{Al}_z\text{Mn}_{2-x-y-z}\text{O}_4$ by the sol-gel method using glutamic acid as the chelating agent.

2. Experimental

LiMn_2O_4 and $\text{LiMg}_x\text{Sn}_y\text{Al}_z\text{Mn}_{2-x-y-z}\text{O}_4$ ($x = 0.01\text{--}0.09$; $y = 0.04\text{--}0.1$; $z = 0.35\text{--}0.20$) powders were synthesized by the sol-gel method. Fig. 1 depicts the flow chart of the synthesis procedure. Stoichiometric amounts of lithium and manganese, nitrates and the dopant salts of magnesium nitrate, aluminum nitrate and tin chloride were combined with one or two drops of concentrated HCl (for dissolution) and dissolved independently in triple-distilled water. The ionic solutions were thoroughly mixed until the solution was homogeneous. The solution was stirred continuously with gentle heating, and 1 M glutamic acid was added drop-wise to allow the chelation to take place. The pH of the solution was maintained between 5 and 6, and the solution was slowly heated until a viscous gel was obtained. This gel mass was dried overnight in a hot air oven at 110°C in order to obtain a dried mass. A small amount of the gel was analyzed using TG/DTA to understand the thermal behavior; the rest of the gel mass was calcined at 850°C for 6 h. For thermal analysis, the precursors were heated at a rate of $10^\circ\text{C min}^{-1}$ up to 850°C in a nitrogen atmosphere. All the calcined samples were subjected to physical characterization studies (X-ray, SEM, TEM, EDAX, XPS, FT-IR) and galvanostatic charge/discharge cycling studies.

2.1. Coin cell fabrication

Coin cells of 2016 configuration were assembled inside an argon filled glove box (MBraun, Germany) using lithium foil as the anode, Celgard 2400 as the separator, 1 M solution of LiPF_6 in a 50:50 (v/v) mixture of ethylene carbonate (EC) and diethylene carbonate (DEC) as the electrolyte and the synthesized material as the cathode. The cathodes were prepared by a slurry coating procedure from a mix comprising the synthesized compound as the cathode active material, carbon black and poly(vinylidene fluoride) (PVdF) binder in *n*-methyl-2-pyrrolidone (NMP) solution. These were mixed in the ratio of 80:10:10 so as to form a slurry. The slurry was coated over aluminum foil and dried in a micro oven at 110°C for 2 h. The dry coating was removed from the oven and pressed under a 10 tonnes load for 2 min, and the cathodes (18 mm diameter) were punched out using a punching machine.

2.2. Electrochemical studies

Coin cells of 2016 configuration were charged/discharged at a constant current of C/10 rate between 2.8 and 5V using an in-house battery cycling unit. The differential capacity curves of

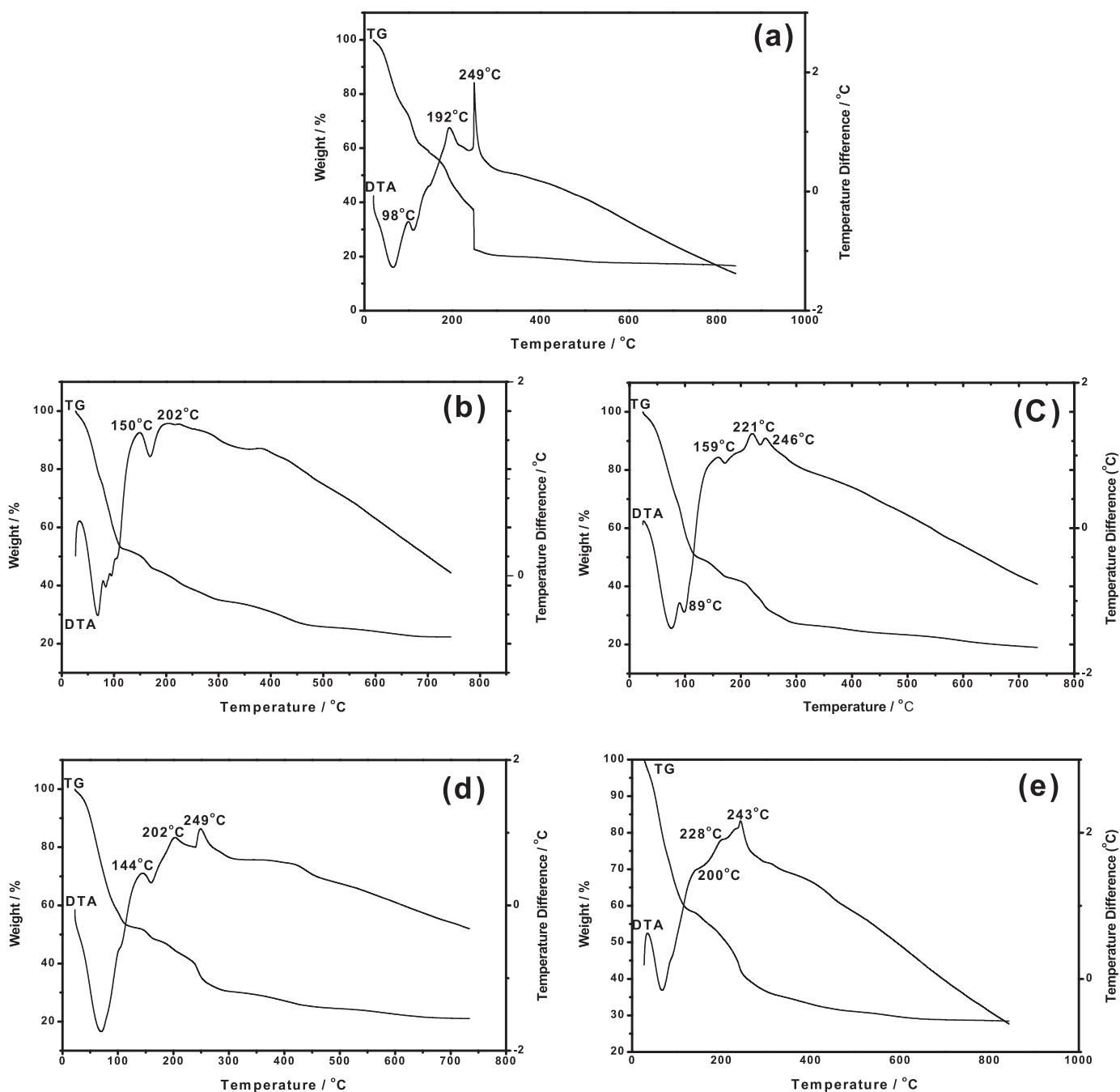


Fig. 2. Thermo gravimetric and differential thermal analysis (TG/DTA) of LiMn_2O_4 and the $\text{LiMg}_x\text{Sn}_y\text{Al}_z\text{Mn}_{2-x-y-z}\text{O}_4$ spinel precursor. (a) Undoped spinel, (b) $x = \text{Mg}-0.01$; $y = \text{Sn}-0.04$; $z = \text{Al}-0.35$, (c) $x = \text{Mg}-0.04$; $y = \text{Sn}-0.06$; $z = \text{Al}-0.30$, (d) $x = \text{Mg}-0.06$; $y = \text{Sn}-0.09$; $z = \text{Al}-0.25$, and (e) $x = \text{Mg}-0.09$; $y = \text{Sn}-0.11$; $z = \text{Al}-0.20$.

LiMn_2O_4 and $\text{LiMg}_{0.01}\text{Sn}_{0.04}\text{Al}_{0.35}\text{Mn}_{1.6}\text{O}_4$ were plotted using the charge–discharge cycling data.

3. Results and discussion

3.1. Thermal studies

Fig. 2(a) shows the TG/DTA curve of the spinel LiMn_2O_4 precursor. The TGA curve depicts four weight loss regions. A weight loss of 25% is observed up to 100 °C, which may be attributed to the removal of water. The weight loss region extending up to 249 °C may be ascribed to the decomposition of precursors and formation of the spinel compound, which is displayed by the predominant exothermic peak observed in the DTA profile. This conclusion is

also corroborated by the XRD profile for the samples calcined at 250 °C, which presented all of the signature peaks of a spinel. The flattening of the DTA curve indicates the closure of thermal events after the formation of spinel products.

Fig. 2(b–e) shows the TG/DTA curve of spinel $\text{LiMg}_x\text{Sn}_y\text{Al}_z\text{Mn}_{2-x-y-z}\text{O}_4$ precursors. In all the cases, the thermal sequences may be categorized into two zones. The first zone, appearing up to 100 °C, may be ascribed to water loss, and it is relatively larger (50%) than that of the undoped spinel precursor. The second zone of events, which occur up to 250 °C, correspond to the decomposition of precursors and the formation of the spinel. The presence of two or more exothermic peaks observed in this zone may be ascribed to the decomposition of multi dopant precursors; the exact identification of these peaks is rather complex.

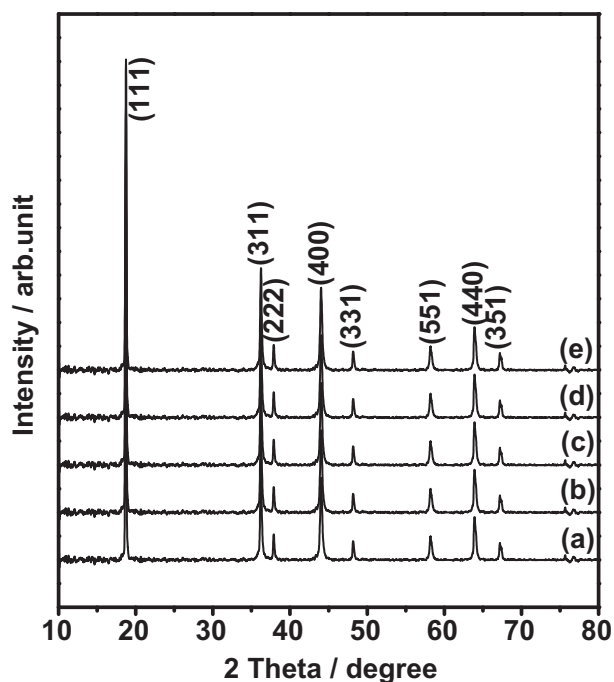


Fig. 3. XRD patterns of undoped spinel and $\text{LiMg}_x\text{Sn}_y\text{Al}_z\text{Mn}_{2-x-y-z}\text{O}_4$ powders calcined at 850°C . (a) Undoped spinel, (b) $x=\text{Mg}-0.01$; $y=\text{Sn}-0.04$; $z=\text{Al}-0.35$, (c) $x=\text{Mg}-0.04$; $y=\text{Sn}-0.06$; $z=\text{Al}-0.30$, (d) $x=\text{Mg}-0.06$; $y=\text{Sn}-0.09$; $z=\text{Al}-0.25$, and (e) $x=\text{Mg}-0.09$; $y=\text{Sn}-0.11$; $z=\text{Al}-0.20$.

All the exothermic peaks observed above 200°C suggest that the product undergoes further crystallization and structural refinement, and the peak at around $243\text{--}249^\circ\text{C}$ confirms the formation of the spinel product. Temperatures beyond 380°C suggest the closure of the thermal events.

3.2. X-ray diffraction studies

Fig. 3 shows the XRD patterns of undoped LiMn_2O_4 and $\text{LiMg}_x\text{Sn}_y\text{Al}_z\text{Mn}_{2-x-y-z}\text{O}_4$. The high intensity XRD reflections corresponding to the (1 1 1), (3 1 1), (2 2 2), (4 0 0), (3 3 1), (5 5 1), (4 4 0) and (3 5 1) planes indicate the formation of a phase pure crystalline spinel that is in line with the results obtained for spinels synthesized through the solid-state-method as well as the sol–gel method [16–25]. All the XRD peak reflections match perfectly with the Joint Committee on Powder Diffraction Standard (JCPDS card No. 35-782).

3.3. FT-IR spectroscopy studies

The FT-IR spectra of sol–gel derived LiMn_2O_4 powders calcined at different temperatures, specifically 250, 450, 650 and 850°C , are shown in **Fig. 4**. The FT-IR spectra of LiMn_2O_4 synthesized either by sol–gel or solid state methods have been reported by several researchers [21,26,27]. IR spectral bands have been observed at wavelengths between $509\text{--}516\text{cm}^{-1}$ and $615\text{--}619\text{cm}^{-1}$ and are ascribed to the Li–O bending vibration and Li–Mn–O stretching vibration, respectively. Further, all the FT-IR peaks for the samples calcined at different temperatures exhibit similar IR spectra. **Fig. 5** depicts the FT-IR spectra of $\text{LiMg}_x\text{Sn}_y\text{Al}_z\text{Mn}_{2-x-y-z}\text{O}_4$ powders with varying amounts of Mg, Sn and Al. In the case of doped spinel compounds, the IR spectral bands observed between $513\text{--}528\text{cm}^{-1}$ and $615\text{--}622\text{cm}^{-1}$ are attributed to the Li–O bending vibration and the reflections at higher wave number correspond to the Li–Mg–Sn–Al–Mn–O stretching vibration. The FT-IR spectra reported for the aluminum doped spinel [18,28] and Mg doped

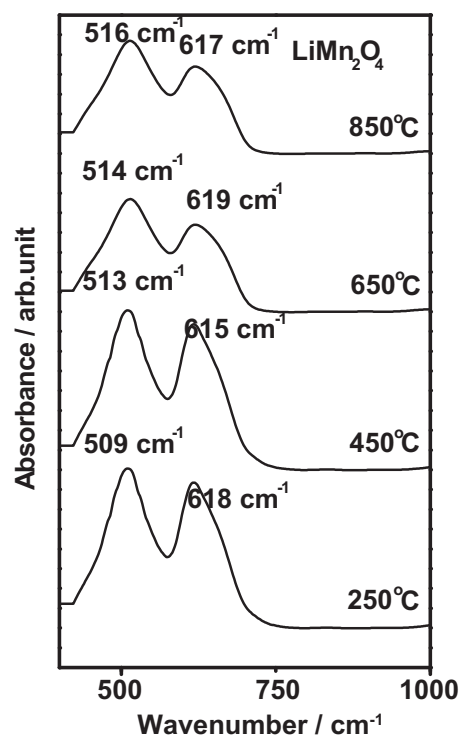


Fig. 4. FT-IR spectra of LiMn_2O_4 particles calcined at different temperatures, specifically 250, 450, 650 and 850°C .

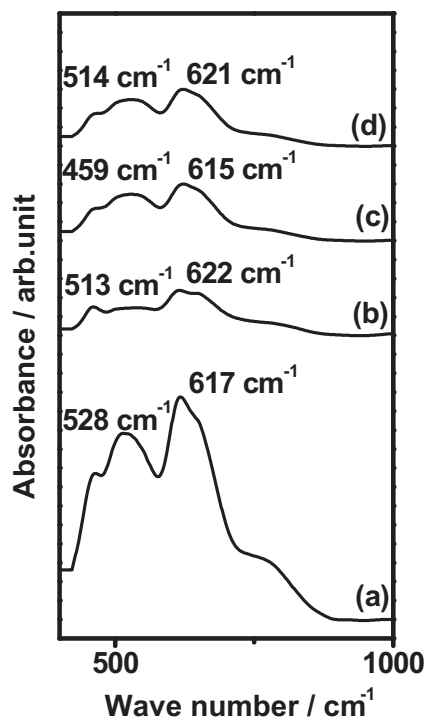


Fig. 5. FT-IR spectra of $\text{LiMg}_x\text{Sn}_y\text{Al}_z\text{Mn}_{2-x-y-z}\text{O}_4$ powders calcined at 850°C . (a) Undoped spinel, (b) $x=\text{Mg}-0.01$; $y=\text{Sn}-0.04$; $z=\text{Al}-0.35$, (c) $x=\text{Mg}-0.04$; $y=\text{Sn}-0.06$; $z=\text{Al}-0.30$, (d) $x=\text{Mg}-0.06$; $y=\text{Sn}-0.09$; $z=\text{Al}-0.25$, and (e) $x=\text{Mg}-0.09$; $y=\text{Sn}-0.11$; $z=\text{Al}-0.20$.

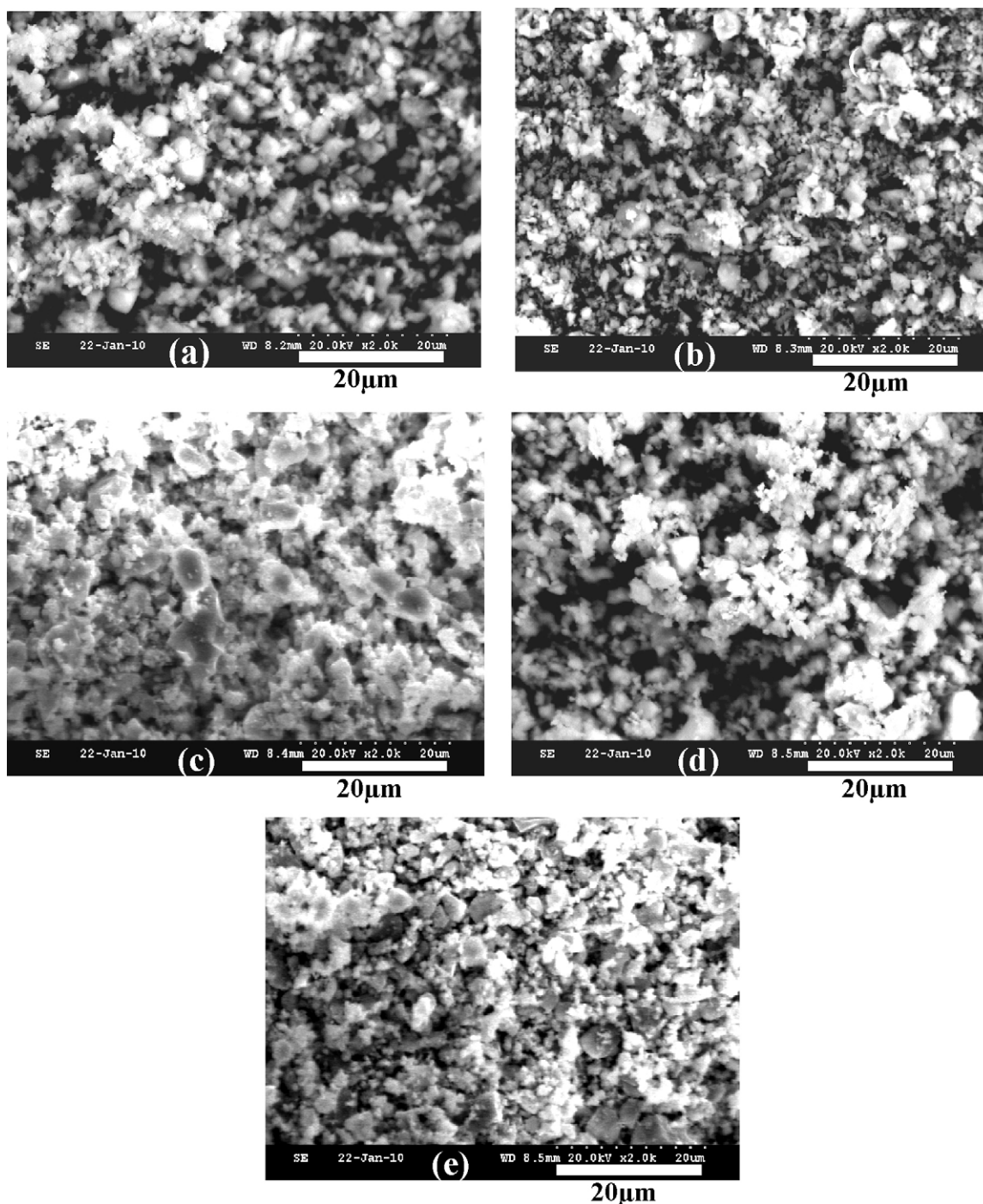


Fig. 6. SEM images of undoped spinel and $\text{LiMg}_x\text{Sn}_y\text{Al}_z\text{Mn}_{2-x-y-z}\text{O}_4$ powders calcined at 850°C . (a) Undoped spinel, (b) $x = \text{Mg}-0.01$; $y = \text{Sn}-0.04$; $z = \text{Al}-0.35$, (c) $x = \text{Mg}-0.04$; $y = \text{Sn}-0.06$; $z = \text{Al}-0.30$, (d) $x = \text{Mg}-0.06$; $y = \text{Sn}-0.09$; $z = \text{Al}-0.25$, and (e) $x = \text{Mg}-0.09$; $y = \text{Sn}-0.11$; $z = \text{Al}-0.20$.

spinel [29] agree with those reported in the present investigation.

3.4. SEM analysis

Fig. 6 depicts SEM images of undoped and doped spinel powders. The undoped spinel (Fig. 6(a)) mostly contains particles less than $1\ \mu\text{m}$ in size. The particles of $\text{LiMg}_{0.01}\text{Sn}_{0.04}\text{Al}_{0.35}\text{Mn}_{1.6}\text{O}_4$ and $\text{LiMg}_{0.04}\text{Sn}_{0.06}\text{Al}_{0.30}\text{Mn}_{1.6}\text{O}_4$ (Fig. 6(b and c)) present a low degree of agglomeration, with a primary particle size of $1\ \mu\text{m}$. Further, the spherical morphology is maintained with higher dopant

concentration (Fig. 6(d and e)), and there is not much variation in the particle size.

3.5. TEM analysis

Fig. 7 shows TEM images of spinel LiMn_2O_4 and $\text{LiMg}_x\text{Sn}_y\text{Al}_z\text{Mn}_{2-x-y-z}\text{O}_4$ particles possessing remarkable porous morphology. The selected area diffraction pattern (Fig. 7(a)) depicts a diffuse hollow with multiple fringes. In the case of $\text{LiMg}_{0.01}\text{Sn}_{0.04}\text{Al}_{0.35}\text{Mn}_{1.6}\text{O}_4$, the particles are loosely agglomerated, which could be beneficial in encapsulating electrolytes. This could in turn result in better diffusion kinetics of Li-ions to

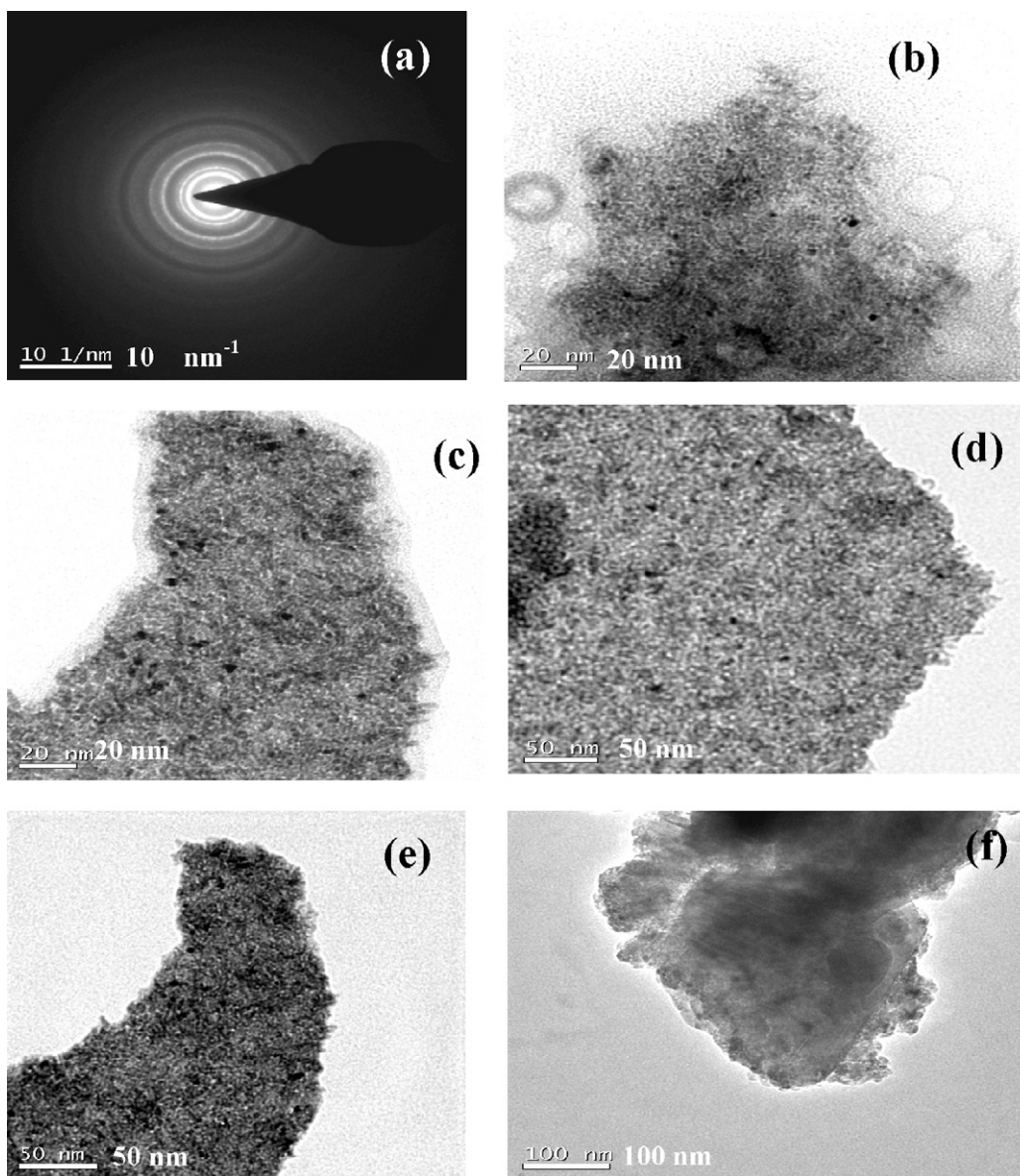


Fig. 7. TEM images of undoped spinel and $\text{LiMg}_x\text{Sn}_y\text{Al}_z\text{Mn}_{2-x-y-z}\text{O}_4$ powders calcined at 850°C . (a) Undoped spinel, (b) $x=\text{Mg}-0.01$; $y=\text{Sn}-0.04$; $z=\text{Al}-0.35$, (c) $x=\text{Mg}-0.04$; $y=\text{Sn}-0.06$; $z=\text{Al}-0.30$, (d) $x=\text{Mg}-0.06$; $y=\text{Sn}-0.09$; $z=\text{Al}-0.25$, and (e) $x=\text{Mg}-0.09$; $y=\text{Sn}-0.11$; $z=\text{Al}-0.20$.

the interfacial locations and could be favorable in deriving better electrochemical performance.

3.6. EDAX analysis

Fig. 8(a–e) depicts the EDAX peaks of Mg, Sn, Al, Mn and O in LiMn_2O_4 and $\text{LiMg}_x\text{Sn}_y\text{Al}_z\text{Mn}_{2-x-y-z}\text{O}_4$ compounds. The EDAX profiles corroborate the exact compositions of the undoped and doped spinels. The unlabeled peaks correspond to zirconium from the zirconia milling pots used for grinding.

3.7. XPS studies

The XPS studies for the undoped LiMn_2O_4 and $\text{LiMg}_{0.01}\text{Sn}_{0.04}\text{Al}_{0.35}\text{Mn}_{1.6}\text{O}_4$ samples have been investigated to understand the oxidation state of metals in the spinel compound synthesized by the sol–gel route. The results are depicted in Figs. 9 and 10, respectively. For the undoped LiMn_2O_4 samples (Fig. 9), the binding energy peaks corresponding to the oxidation

state for Li 1s, Mn 2p, O 1s, and C 1s at 49.7, 642.7, 530.6 and 285.3 eV are well represented. All the XPS reflections agree with those in earlier reports [27]. Fig. 10(c–e) clearly depicts the binding energy of the predominant peaks for the doped spinel, in which the binding energies corresponding to Al 2p, Mg 1s and Sn 3d are assigned to Al^{3+} , Mg^{2+} , Sn^{2+} at 75.4, 1304.7 and 486.7 eV and are in good agreement with earlier reports [28,29].

3.8. Galvanostatic charge–discharge studies

Fig. 11 shows the first cycle charge–discharge behavior of pure LiMn_2O_4 and $\text{LiMg}_x\text{Sn}_y\text{Al}_z\text{Mn}_{2-x-y-z}\text{O}_4$ particles with different Mg, Sn and Al stoichiometry. The charge discharge profiles of both undoped and doped spinels exhibit similar behavior, indicating that doping with multiple cations does not cause any structural modifications or any significant change in the electrochemical sequence. The undoped LiMn_2O_4 spinel synthesized using glutamic acid as the chelating agent and calcined at 850°C delivers a maximum discharge capacity of 122 mAh g^{-1} compared to a theoretical capacity

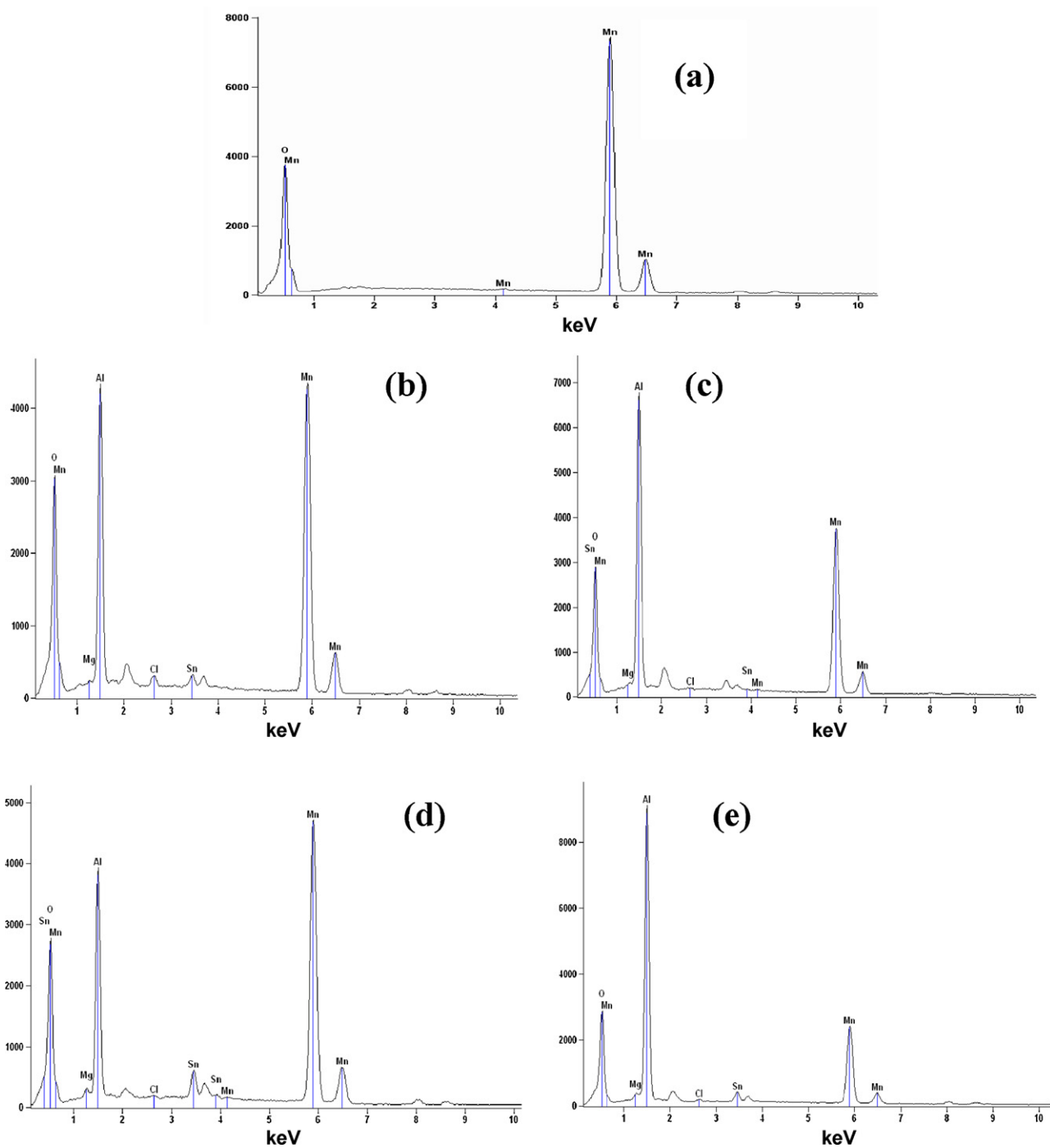
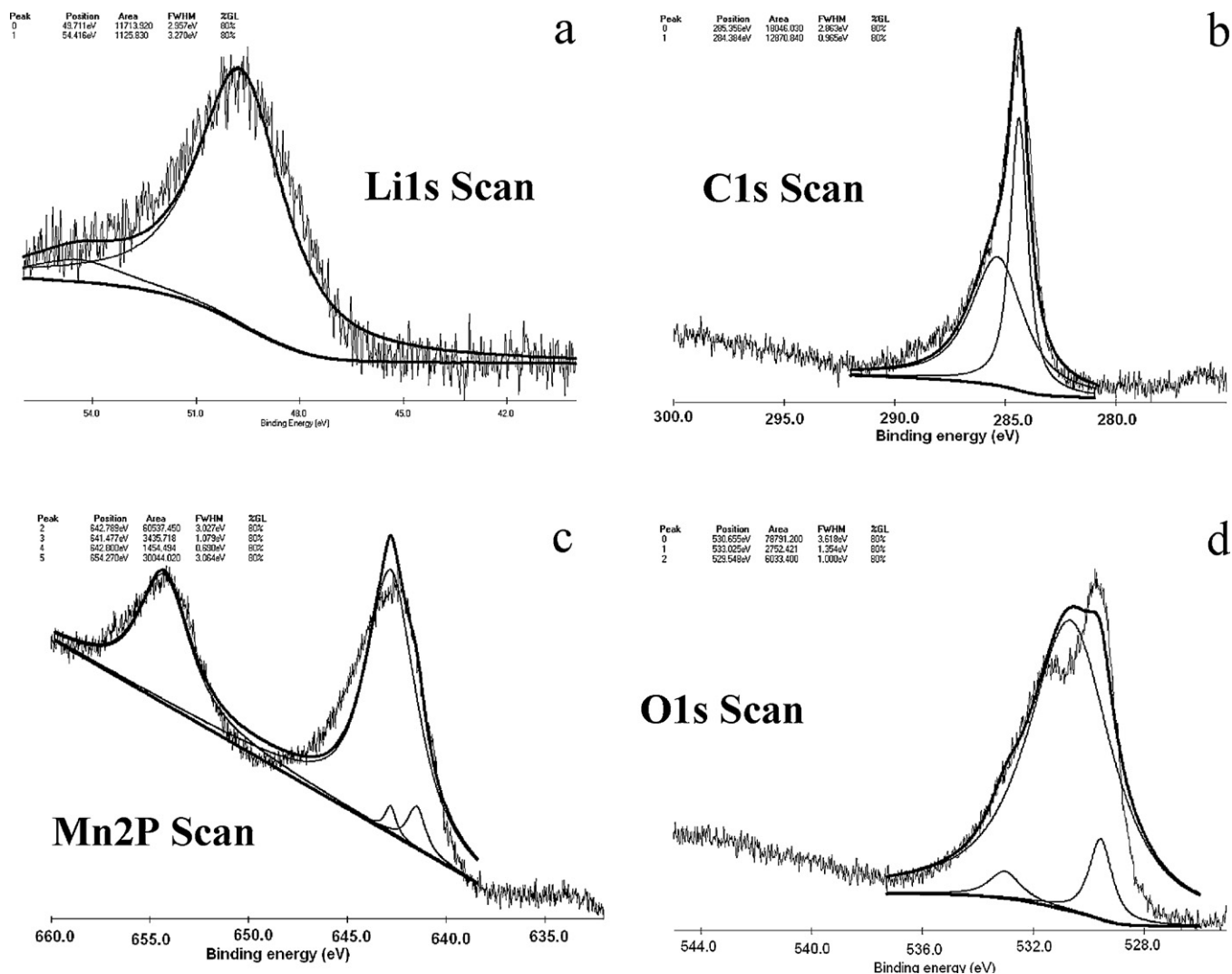


Fig. 8. EDAX images of undoped spinel and $\text{LiMg}_x\text{Sn}_y\text{Al}_z\text{Mn}_{2-x-y-z}\text{O}_4$ powders calcined at 50°C . (a) Undoped spinel, (b) $x=\text{Mg}-0.01$; $y=\text{Sn}-0.04$; $z=\text{Al}-0.35$, (c) $x=\text{Mg}-0.04$; $y=\text{Sn}-0.06$; $z=\text{Al}-0.30$, (d) $x=\text{Mg}-0.06$; $y=\text{Sn}-0.09$; $z=\text{Al}-0.25$, and (e) $x=\text{Mg}-0.09$; $y=\text{Sn}-0.11$; $z=\text{Al}-0.20$.

of 148.6mAhg^{-1} , which corresponds to a 67% material efficiency during the first cycle. The discharge capacity is also higher than that of the doped spinels. Further, these results are superior than those of earlier studies [30] of an undoped spinel synthesized via the sol-gel method, in which a discharge capacity of 98mAhg^{-1} was obtained during the first cycle and 92mAhg^{-1} in 10 cycles. The function of glutamic acid as the chelating agent in synthesizing the spinel compound via the sol-gel method facilitates the formation of a metal ligand chain between $\text{Mn}-\text{O}$ and COO^- , resulting in the formation of a LiMn_2O_4 and $\text{LiMg}_x\text{Sn}_y\text{Al}_z\text{Mn}_{2-x-y-z}\text{O}_4$ spinel product that eventually contributes to a higher discharge performance.

The discharge performance and coulombic efficiency delivered by the undoped and doped spinels over the investigated 10 cycles are depicted in Figs. 12 and 13, respectively. An overview on these graphical representations depicts the fact that undoped and doped spinels (Mg, Al and Sn) of different stoichiometry deliver (Fig. 12) a maximum discharge capacity of 122, 115, 110, 106 and 104mAhg^{-1} during the first cycle respectively. However, in the case of doped samples, it can be seen that the sample with low Mg-doping ($\text{LiMg}_{0.01}\text{Sn}_{0.04}\text{Al}_{0.35}\text{Mn}_{1.6}\text{O}_4$) exhibits a higher capacity (115mAhg^{-1}) than the other compositions. The capacity fade of the undoped and doped samples is on the order 1.6, 1.0, 1.4, 1.5 and $1.4\text{mAhg}^{-1}\text{cycle}^{-1}$ over the investigated 10

Fig. 9. XPS studies of LiMn_2O_4 .

cycles. Thus, $\text{LiMg}_{0.01}\text{Sn}_{0.04}\text{Al}_{0.35}\text{Mn}_{1.6}\text{O}_4$ outperforms the other dopant concentrations and the pristine one in terms of discharge capacity and stable discharge behavior, thereby exhibiting low capacity fading of $1.4 \text{ mAh g}^{-1} \text{ cycle}^{-1}$ over the investigated 10 cycles. This superior performance may be attributed to low order of cation mixing which stabilizes the spinel structure. Further, a comparison of these results with those in the literature indicates that manganese spinels with 0.05 Mg, 0.10 Mg and 0.05 Al doping synthesized by a co-precipitation method [31] have been reported to deliver maximum discharge capacities of 98, 93 and 102 mAh g^{-1} on the 10th cycle, which is inferior to our results. Furthermore, the $\text{LiAl}_{0.05}\text{Mn}_{1.95}\text{O}_4$ spinel has been synthesized by ultrasonic assisted sol-gel method [30] to deliver a maximum discharge capacity of 100 mAh g^{-1} during the 10th cycle. Moreover, it has been claimed that the studies on $\text{LiAl}_{0.1}\text{Mn}_{1.9}\text{O}_4$ [32] stabilized its capacity at approximately 60 mAh g^{-1} after the 5th cycle, which is also lower than our reported results. Therefore, it is apparent from the present investigation on the synthesis of spinel compounds using glutamic acid as the chelating agent achieves better electrochemical stability upon repeated cycling compared to earlier results.

3.9. dQ/dE vs. potential curves

The differential capacity curves plotted from the charge-discharge data of the parent LiMn_2O_4 calcined at 850°C are illustrated in Fig. 14(a). These curves depict redox peaks corresponding to the extraction and insertion of lithium. Two well-defined anodic peaks around 4.03 and 4.16V correspond to the $\text{Mn}^{3+}/\text{Mn}^{4+}$ couples and the two broad reductive peaks at about 3.5 and 3.6V indicate the reductive behavior of the spinel. Moreover, the two anodic peaks of the undoped spinel exhibit high peak currents of 644 and $670 \text{ mAh g}^{-1} \text{ mV}^{-1}$, and the cathodic peaks are relatively broader and show low peak currents; this indicates that the anodic process is more facile than the cathodic one and that the cathodic process is diffusion controlled. Further, the peaks confirm the reversibility of the electrode reaction.

The differential capacity curve of $\text{LiMg}_{0.01}\text{Sn}_{0.04}\text{Al}_{0.35}\text{Mn}_{1.6}\text{O}_4$ calcined at 850°C is shown in Fig. 14(b). The plots show similar behavior to that of the pure sample. A closer observation of the peaks suggests that the positive peak currents give the impression of slight superiority in the reaction scheme, which is eventually reflected in the higher coulombic efficiency upon cycling.

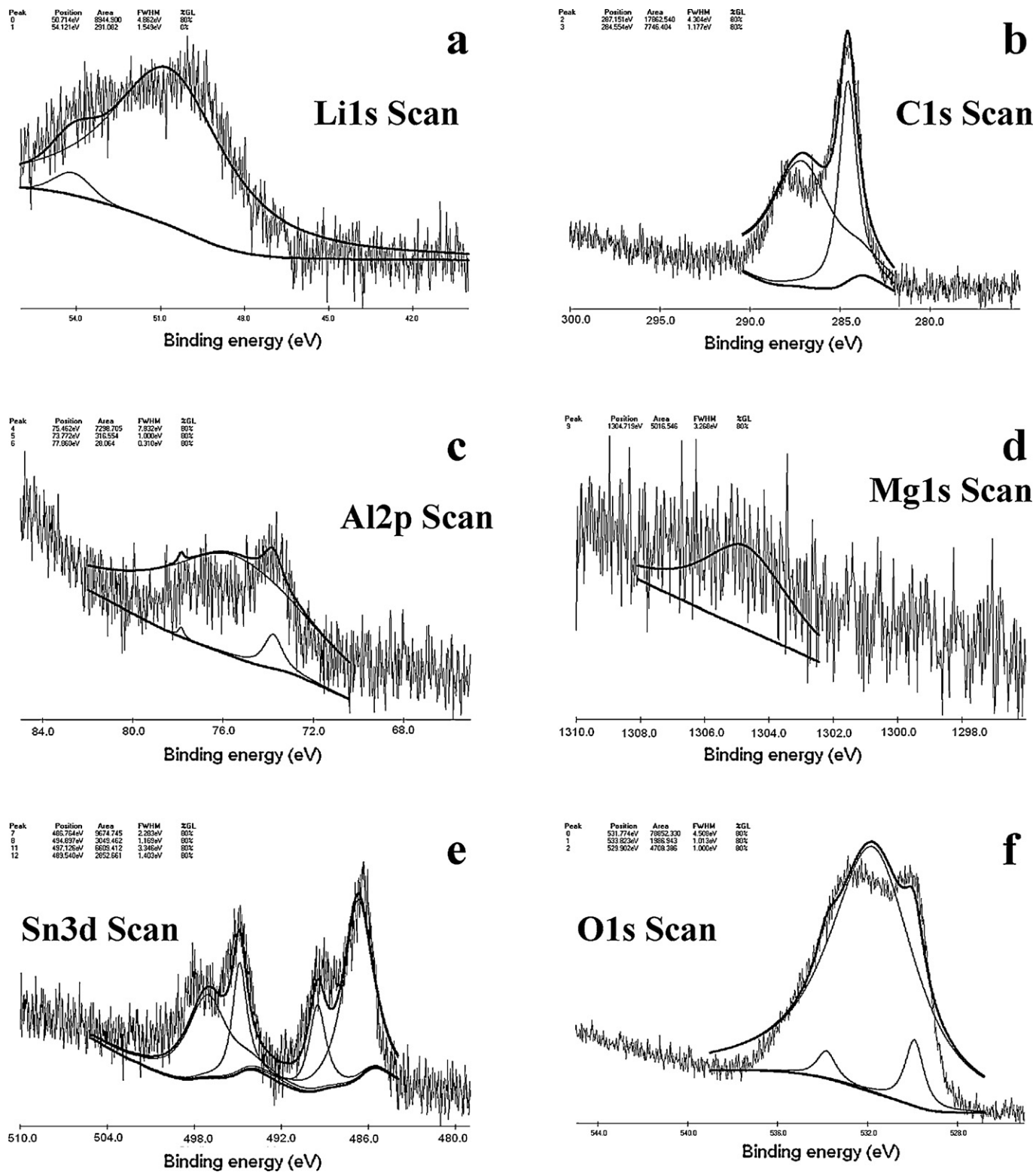


Fig. 10. XPS studies of $\text{LiMg}_x\text{Sn}_y\text{Al}_z\text{Mn}_{2-x-y-z}\text{O}_4$.

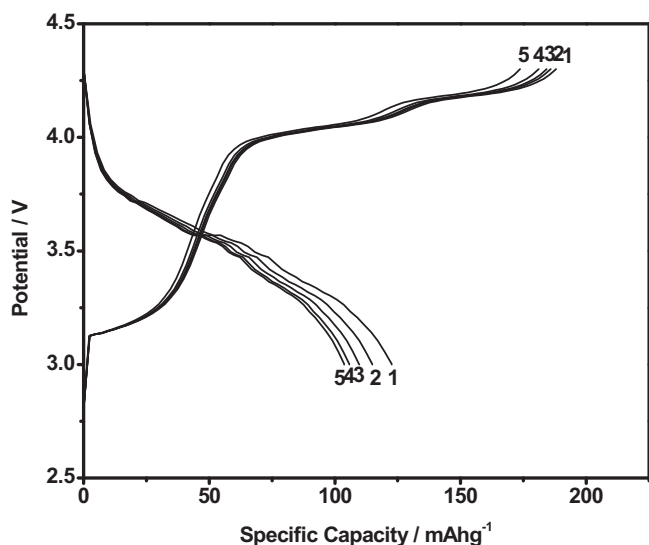


Fig. 11. First cycle charge-discharge behavior of LiMn_2O_4 and $\text{LiMg}_x\text{Sn}_y\text{Al}_z\text{Mn}_{2-x-y-z}\text{O}_4$ particles calcined at 850°C . (1) Undoped spinel, (2) $x = \text{Mg}-0.01$; $y = \text{Sn}-0.04$; $z = \text{Al}-0.35$, (3) $x = \text{Mg}-0.04$; $y = \text{Sn}-0.06$; $z = \text{Al}-0.30$, (4) $x = \text{Mg}-0.06$; $y = \text{Sn}-0.09$; $z = \text{Al}-0.25$, and (5) $x = \text{Mg}-0.09$; $y = \text{Sn}-0.11$; $z = \text{Al}-0.20$.

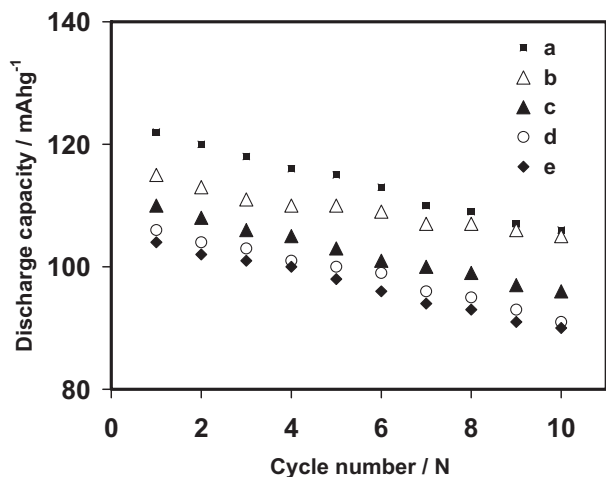


Fig. 12. Discharge capacity of LiMn_2O_4 and $\text{LiMg}_x\text{Sn}_y\text{Al}_z\text{Mn}_{2-x-y-z}\text{O}_4$ particles calcined at 850°C . (a) Undoped spinel, (b) $x = \text{Mg}-0.01$; $y = \text{Sn}-0.04$; $z = \text{Al}-0.35$, (c) $x = \text{Mg}-0.04$; $y = \text{Sn}-0.06$; $z = \text{Al}-0.30$, (d) $x = \text{Mg}-0.06$; $y = \text{Sn}-0.09$; $z = \text{Al}-0.25$, and (e) $x = \text{Mg}-0.09$; $y = \text{Sn}-0.11$; $z = \text{Al}-0.20$.

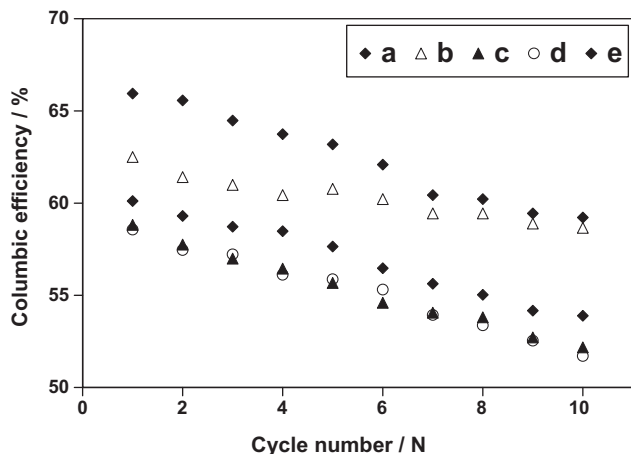


Fig. 13. Columbic efficiency of LiMn_2O_4 and $\text{LiMg}_x\text{Sn}_y\text{Al}_z\text{Mn}_{2-x-y-z}\text{O}_4$ particles calcined at 850°C . (a) Undoped spinel, (b) $x = \text{Mg}-0.01$; $y = \text{Sn}-0.04$; $z = \text{Al}-0.35$, (c) $x = \text{Mg}-0.04$; $y = \text{Sn}-0.06$; $z = \text{Al}-0.30$, (d) $x = \text{Mg}-0.06$; $y = \text{Sn}-0.09$; $z = \text{Al}-0.25$, and (e) $x = \text{Mg}-0.09$; $y = \text{Sn}-0.11$; $z = \text{Al}-0.20$.

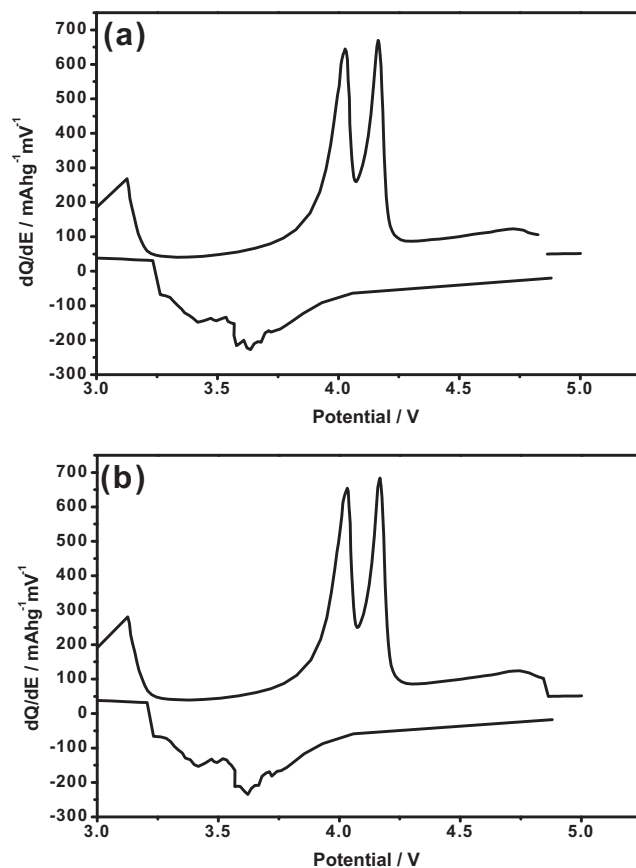


Fig. 14. (a) Differential capacity curve for LiMn_2O_4 and (b) Differential capacity curve for $\text{LiMg}_{0.01}\text{Sn}_{0.04}\text{Al}_{0.35}\text{Mn}_{1.6}\text{O}_4$.

4. Conclusion

For the first time, pure spinel LiMn_2O_4 and $\text{LiMg}_x\text{Sn}_y\text{Al}_z\text{Mn}_{2-x-y-z}\text{O}_4$ ($x, y, z = \text{Mg, Sn, Al}$) ($x = 0.01-0.09$; $y = 0.04-0.1$; $z = 0.35-0.20$) powders have been synthesized by the sol-gel method using glutamic acid as the chelating agent to obtain micron-sized particles for use as cathode materials in lithium rechargeable batteries. All the XRD peak reflections of LiMn_2O_4 and $\text{LiMg}_x\text{Sn}_y\text{Al}_z\text{Mn}_{2-x-y-z}\text{O}_4$ calcined at 850°C reflect a high degree of crystallinity and phase purity of the synthesized materials. The SEM images of the parent LiMn_2O_4 reveal that the majority of the grains are $1\ \mu\text{m}$ in size. The $\text{LiMg}_{0.01}\text{Sn}_{0.04}\text{Al}_{0.35}\text{Mn}_{1.6}\text{O}_4$ and $\text{LiMg}_{0.04}\text{Sn}_{0.06}\text{Al}_{0.30}\text{Mn}_{1.6}\text{O}_4$ particles present a low degree of agglomeration, and the primary particles are $1\ \mu\text{m}$ in size. TEM images of the spinel LiMn_2O_4 and $\text{LiMg}_x\text{Sn}_y\text{Al}_z\text{Mn}_{2-x-y-z}\text{O}_4$ ascertain that the synthesized particles are nano-sized, with uniform surface morphology. EDAX peaks of Mg, Sn, Al, Mn and O have corroborated their exact compositions in LiMn_2O_4 and $\text{LiMg}_x\text{Sn}_y\text{Al}_z\text{Mn}_{2-x-y-z}\text{O}_4$. XPS studies depict the surface oxidation state of the metals in LiMn_2O_4 and $\text{LiMg}_x\text{Sn}_y\text{Al}_z\text{Mn}_{2-x-y-z}\text{O}_4$ compounds. LiMn_2O_4 samples calcined at 850°C deliver a discharge capacity of $122\ \text{mAh g}^{-1}$ in the first cycle. Among the investigation of all dopant concentrations, the $\text{LiMg}_{0.01}\text{Sn}_{0.04}\text{Al}_{0.35}\text{Mn}_{1.6}\text{O}_4$ sample exhibits a stable discharge behavior with a low capacity fade of $1\ \text{mAh g}^{-1}\ \text{cycle}^{-1}$ over the 10 cycles investigated.

Acknowledgement

The authors gratefully acknowledge the support given under the Indo-Taiwan collaborative research program.

References

- [1] J.M. Tarascon, W.R. McKinnon, F. Coowar, T.N. Bowmer, G.G. Amatucci, D. Guyomard, *J. Electrochem. Soc.* 141 (1994) 1431.
- [2] R.J. Gummow, A. de Kock, M.M. Thackeray, *Solid State Ionics* 69 (1994) 67.
- [3] M.M. Thackeray, A. de Kock, M.H. Rossouw, D. Liles, R. Bittihn, D. Hoge, *J. Electrochem. Soc.* 139 (1992) 366.
- [4] Y. Xia, M. Yoshio, Y.H. Zhou, *J. Electrochem. Soc.* 144 (1997) 2600.
- [5] G. Pistoia, A. Antonini, R. Rosati, D. Zane, *Electrochim. Acta* 41 (1996) 2689.
- [6] D.H. Jang, J.Y. Shin, S.M. Oh, *J. Electrochem. Soc.* 143 (1996) 2211.
- [7] A. Yamada, *J. Solid State Chem.* 122 (1996) 165.
- [8] D. Song, H. Ikuta, T. Uchida, M. Wakihara, *Solid State Ionics* 117 (1999) 156.
- [9] M. Javed Iqbal, S. Zahoor, *J. Power Sources* 165 (2007) 397.
- [10] J.H. Lee, J.K. Hong, D.H. Jang, Y.K. Sun, M. Seung, *J. Power Sources* 89 (2000) 14.
- [11] S.H. Park, K.S. Park, Y.K. Sun, K.S. Nahm, *J. Electrochem. Soc.* 147 (2000) 2121.
- [12] S. Bach, M. Henry, N. Baffier, I. Livage, *J. Solid State Chem.* 88 (1990) 333.
- [13] J.P. Perreira-Ramos, *J. Power Sources* 54 (1995) 126.
- [14] P. Barboux, J.M. Tarascon, F.K. Shokoohi, *J. Solid State Chem.* 94 (1991) 196.
- [15] W. Liu, G.C. Farrington, F. Chaput, B. Dunn, *J. Electrochem. Soc.* 143 (1996) 884.
- [16] R. Thirunakaran, N. Kalaiselvi, P. Periasamy, B. Rameshbabu, N.G. Renganathan, N. Muniyandi, *Ionics* 7 (2001) 191.
- [17] S.H. Guo, S.C. Zhang, X.M. He, W.H. Pu, C.Y. Jiang, C.R. Wan, *J. Electrochem. Soc.* 155 (2008) A760.
- [18] R. Thirunakaran, A. Sivashanmugam, S. Gopukumar, C.W. Dunnill, D.H. Gregory, *J. Phys. Chem. Solids* 69 (2008) 2092.
- [19] A. Veluchamy, H. Ikuta, M. Wakihara, *Solid State Ionics* 143 (2001) 171.
- [20] G.T.K. Fey, C.Z. Lu, T. Prem kumar, *Mater. Chem. Phys.* 80 (2003) 318.
- [21] R. Thirunakaran, A. Sivashanmugam, S. Gopukumar, R. Rajalakshimi, *J. Power Sources* 187 (2009) 574.
- [22] R. Thirunakaran, K.-T. Kim, Y.-M. Kang, C.-Y. Seo, J.-Y. Lee, *J. Power Sources* 137 (2004) 104.
- [23] R. Thirunakaran, K.-T. Kim, Y.-M. Kang, C.-Y. Seo, J.-Y. Lee, *Mater. Res. Bull.* 40 (2005) 186.
- [24] R. Thirunakaran, A. Sivashanmugam, S. Gopukumar, C.W. Dunnill, D.H. Gregory, *J. Mater. Process. Technol.* 208 (2008) 531.
- [25] R. Thirunakaran, A. Sivashanmugam, S. Gopukumar, C.W. Dunnill, D.H. Gregory, *Mater. Res. Bull.* 43 (2008) 2129.
- [26] A. Vadivel Murugan, B.B. Kale, B. Lalita Kunde, V. Kulkarni Aarti, *J. Solid State Electrochem.* 10 (2006) 109.
- [27] P. Kalyani, N. Kalaiselvi, N.G. Renganathan, *Mater. Chem. Phys.* 90 (2005) 202.
- [28] P. Singh, A. Sil, M. Nath, Subrata Ray, *Phys. Rev. B: Condens. Matter* 405 (2010) 654.
- [29] Y.K. Yoon, C.W. Park, H.Y. Ahn, D.H. Kim, Y.S. Lee, J. Kim, *J. Phys. Chem. Solids* 68 (2007) 780.
- [30] I.N. Shabanova, V.A. Trapeznikov, *J. Electron. Spectrosc. Relat. Phenom.* 6 (1975) 307.
- [31] B.J. Hwang, R. Santhanam, D.G. Liu, Y.W. Tsai, *J. Power Sources* 102 (2001) 326.
- [32] S.G. Youn, I.H. Lee, C.S. Yoon, C.K. Kim, Y.-K. Sun, Y.-S. Lee, *J. Power Sources* 108 (2002) 105.